

A Comparative Study on the Thermophysical Properties for Two Bis[(trifluoromethyl)sulfonyl]imide-Based Ionic Liquids Containing the Trimethyl-Sulfonium or the Trimethyl-Ammonium Cation in Molecular Solvents

Erwan Couadou,^{†,‡} Johan Jacquemin,[‡] Hervé Galiano,[§] Christopher Hardacre,[‡] and Mérièm Anouti^{*,†}

[†]Université François Rabelais, Laboratoire PCM2E, Parc de grandmont 37200 Tours, France

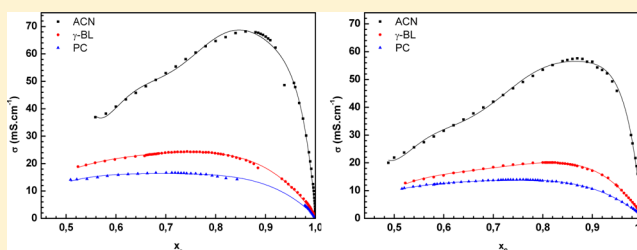
[‡]The QUILL Research Centre, School of Chemistry and Chemical Engineering, Queen's University of Belfast, Stranmillis Road, Belfast BT9 5AG, United Kingdom

[§]CEA, DAM, Le Ripault, F-37260 Monts, France

S Supporting Information

ABSTRACT: Herein, we present a comparative study of the thermophysical properties of two homologous ionic liquids, namely, trimethyl-sulfonium bis[(trifluoromethyl)sulfonyl]imide, $[S_{111}][TFSI]$, and trimethyl-ammonium bis[(trifluoromethyl)sulfonyl]imide, $[HN_{111}][TFSI]$, and their mixtures with propylene carbonate, acetonitrile, or gamma butyrolactone as a function of temperature and composition. The influence of solvent addition on the viscosity, conductivity, and thermal properties of IL solutions was studied as

a function of the solvent mole fraction from the maximum solubility of IL, x_s , in each solvent to the pure solvent. In this case, x_s is the composition corresponding to the maximum salt solubility in each liquid solvent at a given temperature from 258.15 to 353.15 K. The effect of temperature on the transport properties of each binary mixture was then investigated by fitting the experimental data using Arrhenius' law and the Vogel–Tamman–Fulcher (VTF) equation. The experimental data shows that the residual conductivity at low temperature, e.g., 263.15 K, of each binary mixture is exceptionally high. For example, conductivity values up to 35 and 42 $\text{mS}\cdot\text{cm}^{-1}$ were observed in the case of the $[S_{111}][TFSI]$ + ACN and $[HN_{111}][TFSI]$ + ACN binary mixtures, respectively. Subsequently, a theoretical approach based on the conductivity and on the viscosity of electrolytes was formulated by treating the migration of ions as a dynamical process governed by ion–ion and solvent–ion interactions. Within this model, viscosity data sets were first analyzed using the Jones–Dole equation. Using this theoretical approach, excellent agreement was obtained between the experimental and calculated conductivities for the binary mixtures investigated at 298.15 K as a function of the composition up to the maximum solubility of the IL. Finally, the thermal characterization of the IL solutions, using DSC measurements, showed a number of features corresponding to different solid–solid phase transitions, T_{S-S} , with extremely low melting entropies, indicating a strong organizational structure by easy rotation of methyl group. These ILs can be classified as plastic crystal materials and are promising as ambient-temperature solid electrolytes.



INTRODUCTION

Ionic liquids, ILs, have attracted a great deal of attention due to their high thermal stability, good conductivity, non-flammability, wide electrochemical windows, and recyclability.^{1–6} Due to their unique physicochemical properties, these “designer solvents” have been intensively investigated for various applications.^{7–11} Furthermore, their properties can be adjusted by appropriately combining different cations or anions or by introducing different chemical functions into the structure of the ions.^{12–16} ILs can be classified into two groups: protic, PILs, and aprotic ionic liquids, AILs.^{1,17} PILs are synthesized by mixing equimolar quantities of a Brønsted acid with a Brønsted base.^{18–20} The proton transfer from the acid to the base creates proton donor and acceptor sites and can lead to the formation of hydrogen bonds.²⁰ However, to date, PILs have not been studied to the same degree as

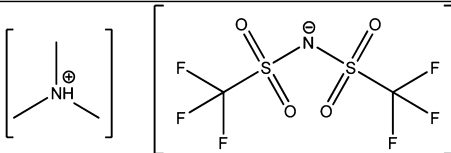
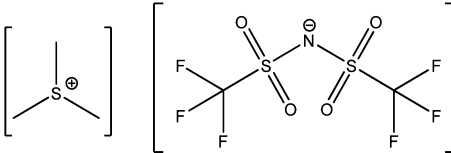
AILs.^{1,21,22} Nevertheless, this IL family has many useful properties and potential applications, often arising from their protic nature, including as self-assembly media,^{23,24} reaction media and catalysts for organic reactions,^{25,26} biological applications,^{27,28} proton conducting electrolytes for polymer membrane fuel cells,^{29,30} and explosives.³¹ In addition, ionic liquids containing ammonium cations have been more extensively studied compared with those based on phosphonium and sulfonium cations, for example. However, sulfonium-based AILs are generating significant interest as potential substitutes for their ammonium counterparts due to practical advantages

Received: August 15, 2012

Revised: December 14, 2012

Published: January 3, 2013

Table 1. Names, Abbreviations, and Structures of Selected ILs

Name	Structure	Abbreviation
Trimethyl-ammonium bis[(trifluoromethyl)sulfonyl]imide		[HN ₁₁₁][TFSI] PIL
Trimethyl-sulfonium bis[(trifluoromethyl)sulfonyl]imide		[S ₁₁₁][TFSI] AIL

including high chemical and electrochemical stabilities.^{32,33} Moreover, sulfonium salts have a range of useful properties that can be applied in specialized areas.³⁴ For example, a recent report indicated that trialkylsulfonium salts based on the dicyanamide anion have lower viscosities in comparison with many other ionic liquids, and are found to be in the range 20–60 mPa·s at 293.15 K.³⁵

Among the most important properties of ILs is their conductivity for potential applications as electrolytes in electrochemical devices. As ILs can be mixed with molecular solvents, this provides new opportunities to study the conductivity of electrolyte solutions in salt-rich regions. There are a large number of studies concerning the specific conductivity and viscosities of pure ILs,^{36–39} since it is desirable and of great importance to understand and predict the transport properties of IL + molecular solvent solutions by using classical and theoretical models.

In this work, we present a comparative study of transport and thermal properties for two pure ILs, the PIL trimethyl-ammonium bis[(trifluoromethyl)sulfonyl]imide and the AIL trimethyl-sulfonium bis[(trifluoromethyl)sulfonyl]imide, as well as their mixtures with three molecular solvents: the gamma-butyrolactone (γ -BL), propylene carbonate (PC), and acetonitrile (ACN) as a function of the composition and temperature from 298.15 to 343.15 K. Experimental measurements of ionic conductivities of binary systems were investigated first at 298.15 K and atmospheric pressure from the limit of solubility of the ILs in each molecular solvent to its infinite dilution region. Furthermore, the temperature effect on the conductivity of the IL solutions at the composition which had the maximum of conductivity at 298.15 K was then quantified for each investigated IL + solvent system from 258.15 to 343.15 K. Additionally, rheological studies were undertaken to compare the viscosity of the pure ILs and their mixtures with selected solvents to investigate the effect of the cation structure, as well as the presence of the solvent. Finally, a theoretical model based on the conductivity and the viscosity of electrolytes has been formulated by treating the migration of ions as a dynamical process governed by ion–ion and solvent–ion interactions. This approach is based on the calculation of viscosity data using the Jones–Dole equation and the determination of the conductivity as a function of composition through the knowledge of the conductivity maximum and viscosity values at the optimum composition. Using this model, excellent agreement with experimental data of each investigated electrolyte up to the composition corresponding to the saturation limit of the ionic liquid was obtained.

1. EXPERIMENTAL SECTION

1.1. Materials. Trimethylsulfonium iodide (99%), trimethylamine ($\geq 99\%$), 37% aqueous solution of hydrochloric acid, anhydrous acetonitrile (99.8%), gamma butyrolactone (99.8%), propylene carbonate (99.9%), and 1,2-dichloroethane (DCE, $>99\%$) were supplied from Sigma-Aldrich. The lithium bis-[(trifluoromethyl)sulfonyl]imide (Li[TFSI], $\geq 99.0\%$) was supplied from Solvionic. All chemicals used during this work were used as received. The water was purified using a Milli-Q 18.3 M Ω water system.

1.2. Methods. All selected binary mixtures were prepared by mass with an accuracy of $\pm 1 \times 10^{-4}$ g using a Sartorius 1602 MP balance. The water content of the ILs was determined before and after measurements by Coulometric Karl Fischer titration using a Mettler Toledo DL31 titrator. The determination of water contents was estimated to be within $\pm 10\%$.

A Crison, GLP 3, digital multifrequency conductometer was utilized to measure the ionic conductivities. The temperature control, from 258.15 to 353.15 K, was realized by a thermostatted bath JULABO F25, with an accuracy of ± 0.2 K. The conductometer was calibrated using standard 0.1 and 0.01 mol·L⁻¹ KCl solutions of known conductivity. The uncertainty of conductivity measurements did not exceed $\pm 2\%$. Each conductivity was recorded after the measurement was stable to within 1% for 2 min.

The rheology of the pure components and their mixtures was determined as a function of temperature from 298.15 to 353.15 K using a TA Instruments rheometer (model AR 1000) with conical geometry. This instrument was fully automated, and therefore, the shear rate and shear stress were automatically fixed and determined, respectively. The temperature in the cell was regulated to ± 0.01 K with a solid-state thermostat. The viscosity standard, Brookfield, 12 700 mPa·s at 298.15 K, and water were used to calibrate the rheometer. From this study, the uncertainty of viscosity measurements did not exceed $\pm 1\%$.

Differential scanning calorimetry, DSC, was carried out on a Perkin-Elmer DSC 4000 under a nitrogen atmosphere, coupled with an Intracooler SP VLT 100. Inert aluminum pans were placed in the measuring cell, containing around 10 mg of studied material, and the reference cell following filling under a N₂ atmosphere.

1.3. Preparation of Selected ILs. The trimethylsulfonium bis[(trifluoromethyl)sulfonyl]imide AIL, [S₁₁₁][TFSI], was synthesized by anionic exchange from I⁻ to [TFSI]⁻ anions by mixing equimolar compositions of [S₁₁₁]I and Li[TFSI] salts in pure water.

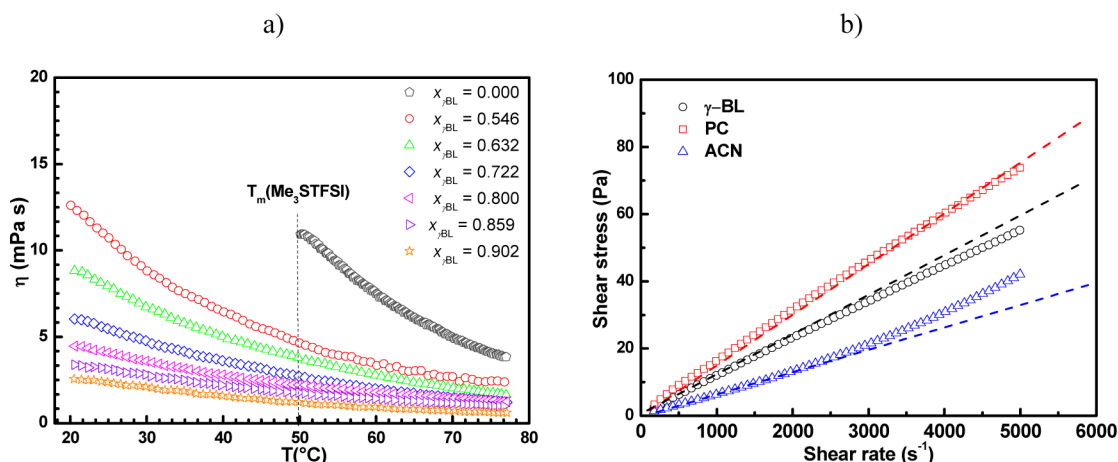


Figure 1. (a) Viscosity measurements of the $[S_{111}][TFSI]$ + γ -BL binary mixture as a function of temperature and γ -BL mole fraction composition. (b) Flow curves for $[S_{111}][TFSI]$ mixed with (○) γ -BL at $x_s = 0.546$, (□) PC at $x_s = 0.524$, and (△) ACN at $x_s = 0.614$; at 293.15 K. The line is just a guide to the eye to show the deviation from Newtonian behavior.

The trimethylammonium bis[(trifluoromethyl)sulfonyl]imide PIL, $[HN_{111}][TFSI]$, was synthesized using a classical two-step IL synthesis procedure. During the first step, the selected cation was formed by mixing dropwise the hydrochloric acid solution with pure trimethylamine under vigorous stirring at 0 °C over 30 min. The trimethylammonium chloride obtained was then mixed with an equimolar aqueous solution of $Li[TFSI]$ under gentle stirring for 2 h to realize the anionic exchange and to form the desired $[HN_{111}][TFSI]$ PIL.

The phase containing the IL, i.e., $[S_{111}][TFSI]$ or $[HN_{111}][TFSI]$, was washed several times with pure water to remove lithium iodide or chloride trace until no $AgNO_3$ precipitation was observed in the washings. The residual water was removed using a water–DCE heteroazeotropic distillation. Residual DCE was finally evaporated under reduced pressure, giving, in each case, a white solid compound with a melting temperature, T_m , of 49.3 and 84.2 °C for $[S_{111}][TFSI]$ and $[HN_{111}][TFSI]$, respectively. Prior to use, pure ILs were dried overnight at high vacuum (1 Pa) at 363.15 K. After this treatment, 600 and 1000 ppm water was found in $[S_{111}][TFSI]$ AIL and $[HN_{111}][TFSI]$ PIL, respectively. The names, abbreviations, and structures of the ILs used in this study are listed in Table 1. ILs were characterized by 1H and ^{13}C NMR spectrometry using a Bruker 200 MHz spectrometer using DMSO as the solvent and TMS as the internal standard. 1H and ^{13}C NMR spectra of the $[S_{111}][TFSI]$ and of $[HN_{111}][TFSI]$ are presented in Figures S1 and S2 of the Supporting Information, respectively.

2. RESULTS AND DISCUSSION

2.1. Rheological Properties of Selected ILs and Mixtures. Since ILs are generally more viscous than conventional solvents, in most applications they are used in mixtures with other less viscous fluids. Therefore, prior to developing any industrial process, an accurate knowledge of the viscosity of pure ILs and their mixtures with conventional solvents is essential. The IL viscosities typically range from 30 to 100 mPa·s at room temperature, although values up to 1000 mPa·s have been reported.⁴⁰ The viscosity is influenced by several parameters. With respect to the anion, a higher basicity, size, and capacity to form hydrogen bonds increase the viscosity of ILs. Moreover, due to the acid/base character of PILs, their viscosity is highly dependent on hydrogen bonds between ions. With respect to the

cation, van der Waals interactions and the size of the cation⁴¹ significantly influence the IL viscosity. In general, the viscosity of sulfonium-based ILs, with the exception of halide salts, is low and, not surprisingly, dependent on the anion structure. At 298.15 K, several asymmetric trialkylsulfonium-based ILs have been reported to have a low viscosity.^{42,43} At 298.15 K, viscosities of ~52 and 66 mPa·s have been reported in the case of dimethyl-ethyl-sulfonium bis[(trifluoromethyl)sulfonyl]imide, $[S_{112}][TFSI]$, and of dimethyl-butyl-sulfonium bis[(trifluoromethyl)sulfonyl]imide, $[S_{114}][TFSI]$, respectively. More surprisingly, viscosities of ~30 mPa·s were reported at 298.15 K, in the case of methyl-diethyl-sulfonium bis[(trifluoromethyl)sulfonyl]imide, $[S_{122}][TFSI]$ (36 mPa·s), triethyl-sulfonium bis[(trifluoromethyl)sulfonyl]imide, $[S_{222}][TFSI]$ (33 mPa·s), propyl-diethyl-sulfonium bis[(trifluoromethyl)sulfonyl]imide, $[S_{322}][TFSI]$ (33 mPa·s), and methyl-ethyl-propyl-sulfonium bis[(trifluoromethyl)sulfonyl]imide, $[S_{123}][TFSI]$ (39 mPa·s).^{42,43} In the present work, the viscosity of $[S_{111}][TFSI]$ and of $[HN_{111}][TFSI]$ was not measured at 298.15 K, since these ILs are solid below 322.45 and 357.35 K, respectively. The viscosity at 298.15 K of the homologous PIL, $[HN_{222}][TFSI]$, has been previously reported to be ~39 mPa·s.⁴⁴ This value is similar to that value reported for the $[S_{222}][TFSI]$ ⁴³ (33 mPa·s at 298.15 K). Both sulfonium AIL and ammonium PIL structures have lower viscosities than those reported for pyrrolidinium or imidazolium based $[TFSI]^-$ ILs which have viscosities generally between 50 and 100 mPa·s at 298.15 K.⁴⁵ In the case of the sulfonium-based IL, $[S_{111}][TFSI]$, investigated, its viscosity is found to be ~11 and 3 mPa·s at 323.15 and 353.15 K, as shown in Figure 1a.

The influence of the addition of the solvent, ACN, γ -BL, and PC, on the rheological properties of ILs was then investigated as a function of temperature from 293.15 to 353.15 K and of the IL mole fraction composition from the maximum solubility of IL, x_s , in each solvent to the pure solvent. Therein, x_s is the composition corresponding to the maximum ionic liquid solubility in each liquid solvent at a given temperature. For all the binary mixtures studied, we initially investigated the relationship between the shear stress and the shear rate, as shown in Figure 1b, for example in the case of $[S_{111}][TFSI]$ in a binary solution with γ -BL, PC, and ACN at 293.15 K and at the mole fraction $x_s = 0.546$, 0.524 , and 0.614 , respectively. The flow curves have different behavior according to the nature of the added solvent. In the case of

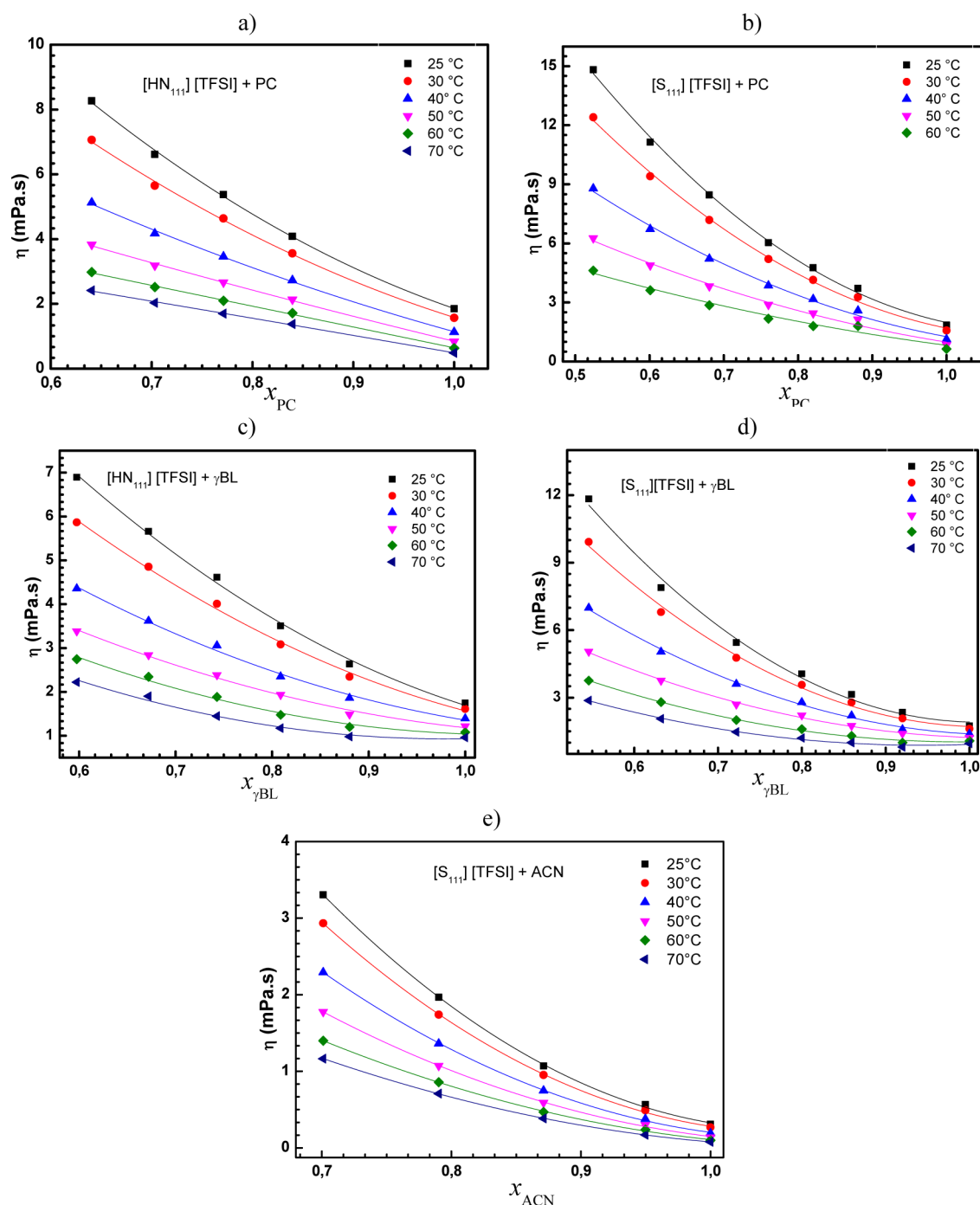


Figure 2. Viscosity of (a) $[\text{HN}_{111}][\text{TFSI}] + \text{PC}$, (b) $[\text{S}_{111}][\text{TFSI}] + \text{PC}$, (c) $[\text{HN}_{111}][\text{TFSI}] + \gamma\text{-BL}$, (d) $[\text{S}_{111}][\text{TFSI}] + \gamma\text{-BL}$, and (e) $[\text{S}_{111}][\text{TFSI}] + \text{ACN}$ binary mixtures at various temperatures as a function of the solvent mole fraction.

solutions containing PC, as shown in Figure 1b, Newtonian behavior, i.e., the shear stress/shear rate ratio is constant, is observed, since the shear stress increases monotonically with the shear rate up to a shear rate close to 5000 s^{-1} . In the case of solutions containing $\gamma\text{-BL}$ or ACN, negative and positive deviations from the Newtonian behavior were observed corresponding to non-Newtonian shear thinning and shear thickening behavior, respectively. In both cases, a shear rate value of 3000 s^{-1} corresponds to the onset of the shear thinning or thickening. Furthermore, it appears that the flow behavior of the investigated mixtures changes from Newtonian to non-Newtonian by changing the nature of the solvent, its composition

from $x_s = 0.546$ to 0.902 , as well as the nature of the selected ILs as exemplified in Figure S3 of the Supporting Information in the case of binary mixtures containing $[\text{HN}_{111}][\text{TFSI}]$. From these data, it appears that $[\text{HN}_{111}][\text{TFSI}] + \text{PC}$ and $[\text{HN}_{111}][\text{TFSI}] + \gamma\text{-BL}$ binary mixtures have also a non-Newtonian behavior starting from a shear rate of 2000 s^{-1} corresponding in each case to the onset of their shear thinning behavior. Herein, all viscosity data reported were measured at a shear rate value close to 500 s^{-1} , since each mixture studied has a Newtonian behavior at this value.

Figure 1a shows, as an example, the viscosity of $[\text{S}_{111}][\text{TFSI}] + \gamma\text{-BL}$ as a function of the temperature and the composition.

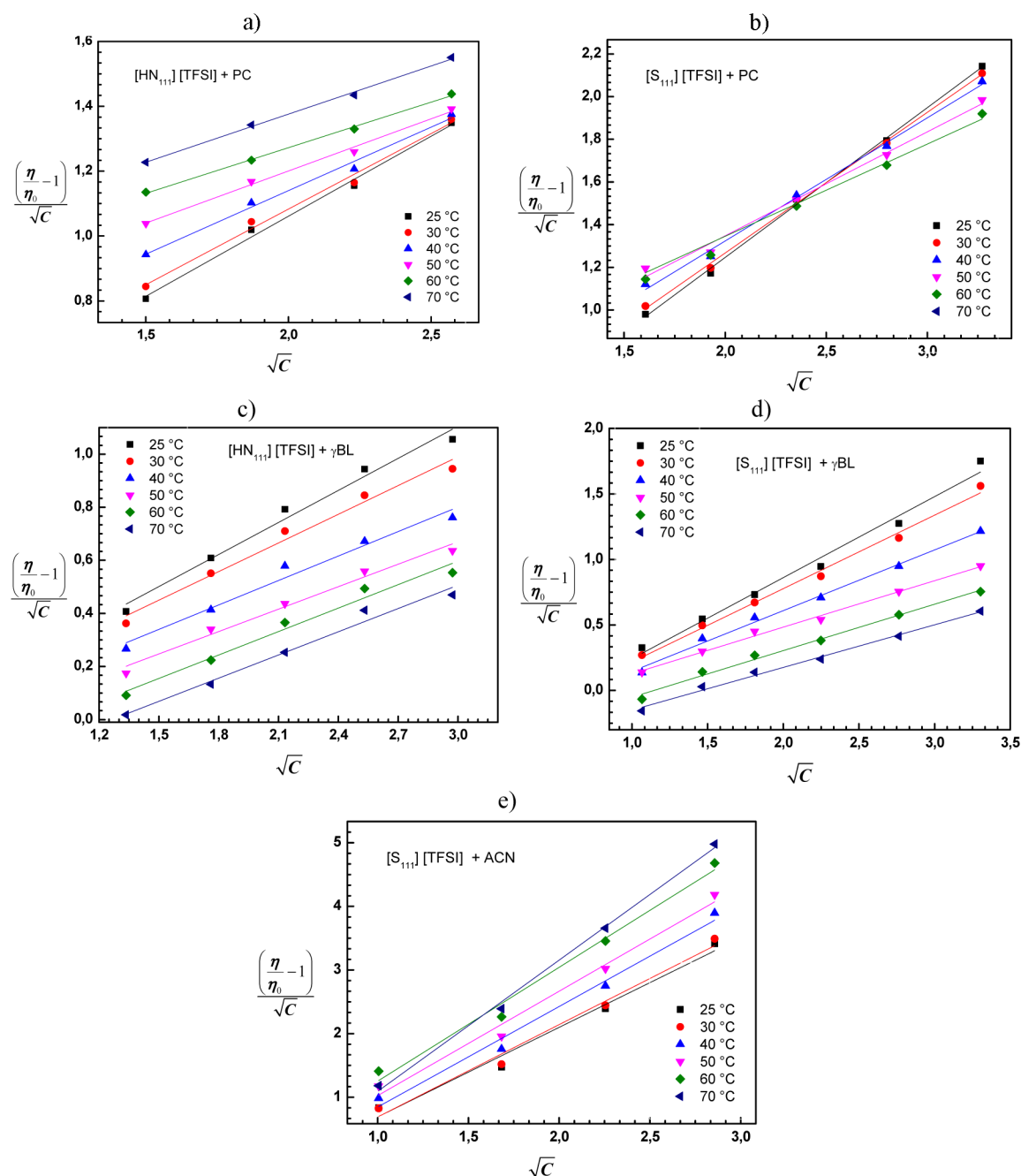


Figure 3. Plot of $((\eta/\eta_0) - 1)/\sqrt{C}$ versus \sqrt{C} of (a) $[\text{HN}_{111}][\text{TFSI}] + \text{PC}$, (b) $[\text{S}_{111}][\text{TFSI}] + \text{PC}$, (c) $[\text{HN}_{111}][\text{TFSI}] + \gamma\text{-BL}$, (d) $[\text{S}_{111}][\text{TFSI}] + \gamma\text{-BL}$, and (e) $[\text{S}_{111}][\text{TFSI}] + \text{ACN}$ as a function of the IL concentration, C , and at different temperatures.

Figures S4 and S5 (Supporting Information) show the analogous viscosity trends in the case of $[\text{S}_{111}][\text{TFSI}] + \text{PC}$ or ACN and $[\text{HN}_{111}][\text{TFSI}] + \text{PC}$ or $\gamma\text{-BL}$, respectively, and the data for all the studied mixtures and temperatures is summarized in Table S1 of the Supporting Information.

Figure 2 illustrates the variation of the viscosity, η , as a function of the temperature from 298.15 to 343.15 K and the solvent mole fraction, x_s , in the case of solutions of PC (Figure 2a and b) and of $\gamma\text{-BL}$ (Figure 2c and d) with the PIL and the AIL, respectively, as well as in the case of the ACN + AIL binary mixture (Figure 2e). It can be observed that there is a regular incremental change in the viscosity of the solution on increasing the IL concentration at a fixed temperature with the viscosity increasing with IL mole fraction, as expected.

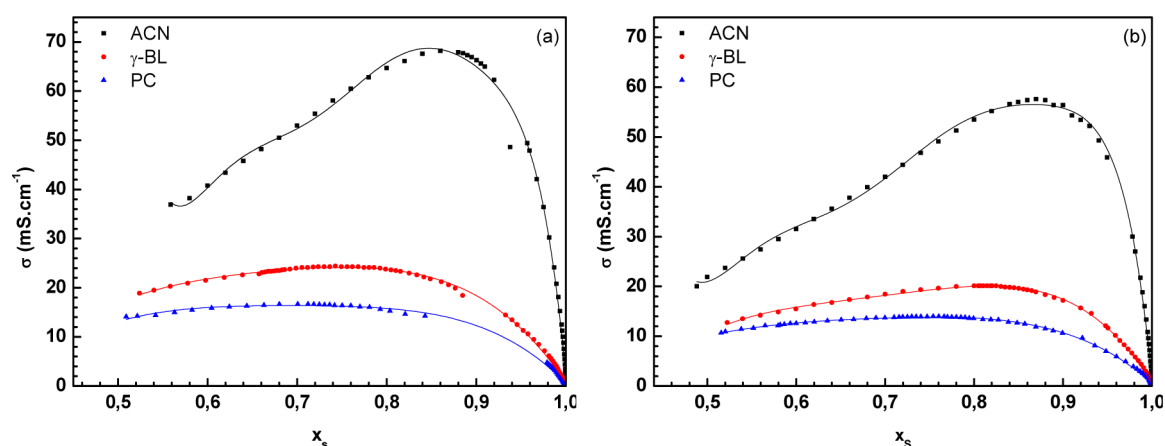
The viscosity of electrolytes varies with concentration C according to the Jones–Dole equation:⁴⁶

$$\frac{\eta}{\eta_0} = 1 + A\sqrt{C} + BC \quad (1)$$

where η and C are the viscosity and concentration of solution and η_0 viscosity of the solvent. A and B are Jones–Dole coefficient values, deduced from Figure 3 as the slope (B) and ordinate (A) from a plot of the reduced viscosity $((\eta/\eta_0) - 1)/\sqrt{C}$ versus \sqrt{C} in the case of solutions of PC (Figure 3a and b) and of $\gamma\text{-BL}$ (Figure 3c and d) containing the PIL or the AIL, respectively, as well as in the case of the ACN + AIL binary mixture (Figure 3e). A is generally independent of concentration, C , and B is related to the effect of the ions on the structure of solvent. B is generally

Table 2. *A* and *B* Jones–Dole Coefficient Calculated from eq 1 and Viscosity Data of $[S_{111}][TFSI]$ AIL and $[HN_{111}][TFSI]$ PIL Solutions with Molecular Solvents as a Function of the Temperature

<i>T</i> (K)	<i>A</i> (mol·L) ^{−1/2}	<i>B</i> (mol·L ^{−1})	<i>A</i> (mol·L) ^{−1/2}	<i>B</i> (mol·L ^{−1})	<i>A</i> (mol·L) ^{−1/2}	<i>B</i> (mol·L ^{−1})
	$[S_{111}][TFSI] + \gamma\text{-BL}$		$[S_{111}][TFSI] + PC$		$[S_{111}][TFSI] + ACN$	
298.15	0.618	−0.376	0.702	−0.157	1.406	−0.714
303.15	0.561	−0.344	0.659	−0.005	1.450	−0.759
313.15	0.463	−0.318	0.557	0.168	1.582	−0.738
323.15	0.355	−0.227	0.487	0.374	1.641	−0.616
333.15	0.355	−0.406	0.470	0.373	1.789	−0.538
343.15	0.325	−0.475			2.069	−0.971
	$[HN_{111}][TFSI] + \gamma\text{-BL}$		$[HN_{111}][TFSI] + PC$			
298.15	0.378	−0.09	0.493	0.074		
303.15	0.338	−0.085	0.466	0.151		
313.15	0.289	−0.114	0.392	0.356		
323.15	0.265	−0.165	0.322	0.557		
333.15	0.277	−0.269	0.281	0.710		
343.15	0.274	−0.346	0.296	0.783		

**Figure 4.** Conductivity of (a) $[S_{111}][TFSI]$ and (b) $[HN_{111}][TFSI]$ in mixtures with (■) ACN, (●) $\gamma\text{-BL}$, and (▲) PC as a function of the solvent mole fraction, x_s , at 298.15 K.

interpreted as a measure of the structure-forming and structure-breaking capacity of an electrolyte in solutions.⁴⁶ A positive value of the *B* coefficient indicates a structure-forming effect, and a negative value shows a structure-breaking effect.⁴⁷

The viscosity data for the mixtures studied have been analyzed using the Jones–Dole equation. The values of *A* and *B* calculated from eq 1 for binary solutions of $[S_{111}][TFSI]$ and $[HN_{111}][TFSI]$ in $\gamma\text{-BL}$, PC, and ACN are summarized in Table 2. From this table, it is clear that the values of *B* are negative for all IL solutions in $\gamma\text{-BL}$ and in ACN. For $[HN_{111}][TFSI] + PC$ solutions, the values of *B* are positive. Furthermore, it also appears from Table 2 that the values of *B* increase with increasing temperature. These results can then be interpreted as a structure-breaking effect on the addition of these ILs to $\gamma\text{-BL}$ and ACN and as a structure-forming effect on the addition of these ILs to PC. In the same solvent, this effect is more pronounced with the $[S_{111}][TFSI]$ than with the $[HN_{111}][TFSI]$. Therefore, the structure-forming capability of the sulfonium cation is higher than that observed for the equivalent ammonium IL. This is probably due to the size of the sulfonium cation and to the fact that the sulfur d-orbitals may be able to interact with solvent through a coordinative bond. Finally, for each salt, the values of *B* vary in the following order according to the nature of the solvent: PC > $\gamma\text{-BL}$ > ACN.

2.1.1. Conductivity Measurements of Selected ILs and Mixtures. Parts a and b of Figure 4 show the change in

conductivity following the addition of the solvents to $[S_{111}][TFSI]$ and $[HN_{111}][TFSI]$ at 298.15 K, respectively. The conductivity, σ , and equivalent molar conductivity, $\Lambda = \sigma/C$, data are presented in Tables S2 and S3 in the Supporting Information as a function of solvent mole fraction, x_s , for each temperature and mixture based on the three solvents and the two ILs studied, therein. From this data, it can be seen that the conductivity of each binary mixture increases quickly to reach a maximum conductivity in the solvent-rich region. For example, maximum conductivities of 58 and 69 mS·cm^{−1} were observed at a solvent mole fraction, x_s , of ~ 0.86 in the case of ACN solutions containing $[S_{111}][TFSI]$ (Figure 4a) and $[HN_{111}][TFSI]$ (Figure 4b) at 298.15 K, respectively. Furthermore, it appears that all mixtures containing ACN have a higher conductivity than those based on the $\gamma\text{-BL}$, since, at 298.15 K, conductivity maxima of 21 and 25 mS·cm^{−1} were obtained at $x_s \approx 0.74$ and 0.80 in the case of $\gamma\text{-BL}$ solutions containing $[S_{111}][TFSI]$ (Figure 4a) and $[HN_{111}][TFSI]$ (Figure 4b), respectively. All PC solutions investigated showed the lowest conductivities, at 298.15 K. For example, maximum conductivities of 14 and 17 mS·cm^{−1} were observed at $x_s \approx 0.70$ and 0.76 for mixtures of $[S_{111}][TFSI] + PC$ (Figure 4a) and $[HN_{111}][TFSI] + PC$ (Figure 4b), respectively. In all cases, at higher mole fractions, the conductivity dropped rapidly to 0 mS·cm^{−1}, since all the pure solvents are insulators. The observed shape of the conductivity curve as a function of the solvent mole fraction follows the same trend as observed

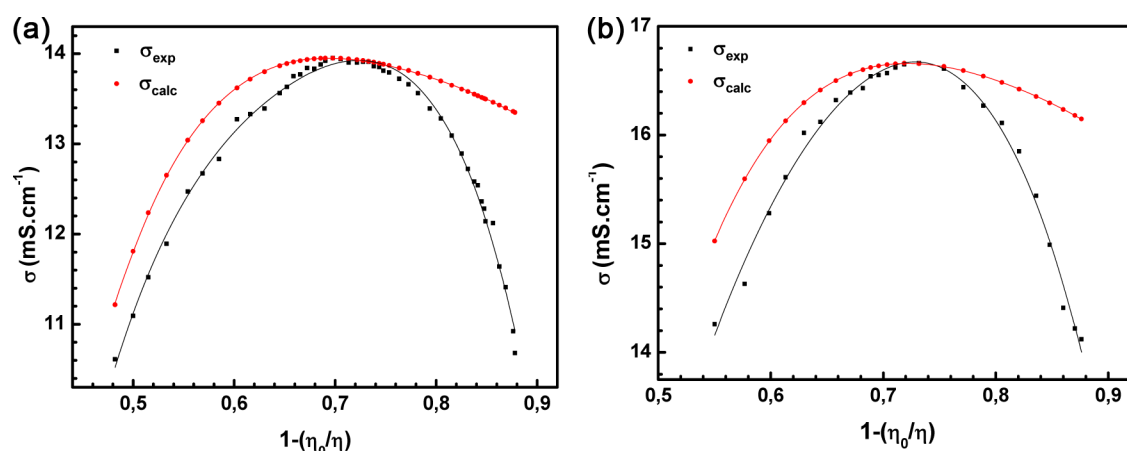


Figure 5. Experimental (σ_{exp}) and calculated (σ_{calc}) specific conductivities as a function of viscosity of (a) $[\text{S}_{111}][\text{TFSI}] + \text{PC}$ and (b) $[\text{HN}_{111}][\text{TFSI}] + \text{PC}$ binary mixtures at 298.15 K.

previously for binary mixtures of ILs with molecular solvents.^{48,49} On the basis of these six investigated binary mixtures, the $[\text{HN}_{111}][\text{TFSI}]$ PIL have higher conductivities compared with those based on the $[\text{S}_{111}][\text{TFSI}]$ AIL. This may be due to the contribution of labile hydrogen driven by the Grotthuss mechanism.³⁹

The similarity between the graphs $\sigma = f(x_s)$ reported for both ILs in Figure 4a and b indicates that the mechanisms of the charge transport must be similar for all investigated IL + solvent binary mixtures. When solvent is added to an IL, the charge density is reduced, as well as the viscosity of the solution. At solvent concentrations close to the maximum conductivity, the effect of dilution by the solvent is dominant.

To the best of our knowledge, a satisfactory quantitative theoretical explanation of the conductivity shape as a function of the composition as well as the localization of the maximum conductivity as a function of the salt structures in different aqueous or non-aqueous solutions does not exist, even in electrolyte solution transport theory. Some studies have provided qualitative explanations based on the presence of a glass transition in the aqueous solution at concentrations at the maximum conductivity.⁵⁰ Vila et al. have shown that, in ionic conduction, two different mechanisms are present.⁵¹ One is dependent on the number of ions present to transport the charge which increases with the IL concentration in solution. The other is related to the ion mobility in the solution, which will be lower when the number of ions increases. This decreases with the IL concentration. At the maximum conductivity, both effects are optimized.^{51,52} However, further increases in the ion concentration results in a sufficiently high number of particles per unit volume, leading to ion–ion interactions and, in the extreme case, ion cluster formation which eventually results in a decrease in the specific conductivity of the solution. Since electrostatic forces vary as the inverse square of the distance between the charges, as the mean distance between ions decreases, the mobility of the ions also decreases. Thus, the conductivity–concentration curves show a maximum that arises from the competition between the increase of conductivity produced by the increase in the concentration of charge carriers and the decrease of ionic mobility as the concentration increases. It should be noted that the variation of mobility with concentration can also be rationalized by the increase in the viscosity of the solution.⁵³

The viscosity is a variable that could describe the effects of dissipation and feedback involved in ion transport more

adequately than the concentration because the viscosity also reflects the nature of the electrolyte. Thus, a change in viscosity produced, for example, by a variation in concentration more properly reflects changes linked to the charge density and to viscous forces. Despite the great importance of ion transport, most of the widely accepted models and theories are valid only in the solvent-rich region, mainly driven by the salt solubility limit in different solvents.^{52,54} Several empirical equations are available in the literature in order to describe the variation of conductivity in a solution based on its concentration and its viscosity. For example, Villullas and Gonzalez⁵⁵ proposed eq 2 in order to calculate a theoretical conductivity curve using experimental values of viscosity and the maximum conductivity, σ_{max} , obtained from the prior study of the conductivity as a function of the composition, as well as the viscosity at this conductivity maximum composition, η_{max} (Table 4), and the viscosity of the pure solvent, η_0 .

$$\sigma = \frac{2\sigma_{\text{max}}}{\left(1 - \frac{\eta_0}{\eta}\right)} \left(1 - \frac{\eta_0}{\eta_{\text{max}}}\right) \left[1 - \frac{1}{2\left(1 - \frac{\eta_0}{\eta}\right)} \left(1 - \frac{\eta_0}{\eta_{\text{max}}}\right)\right] \quad (2)$$

This means that, if the experimental values of σ_{max} and η_{max} are available, it is then possible to predict the variation of the conductivity as a function of the composition for a given temperature. The calculated conductivity values in the case of the PC solutions containing the selected sulfonium-based AIL and ammonium-based PIL are shown in Figure 5a and b, respectively. These figures also provide a comparison of experimental data with those calculated using eq 2. The experimental data set of each electrolyte used during this work is tabulated in Table S3 of the Supporting Information. This comparison shows that eq 2 is fully adequate to describe the mutual dependencies between the specific conductivity, the viscosity, and, indirectly, the concentration of the electrolyte solution at a given temperature at the maximum conductivity. The agreement shown using eq 2 is impressive due to its simple form and the basic approach proposed herein, i.e., as a quadratic equation based only on one variable.

The molar conductivities, Λ , of the ILs in the different solutions were then calculated from the experimental ionic conductivities at the IL molar concentrations, C_{IL} :

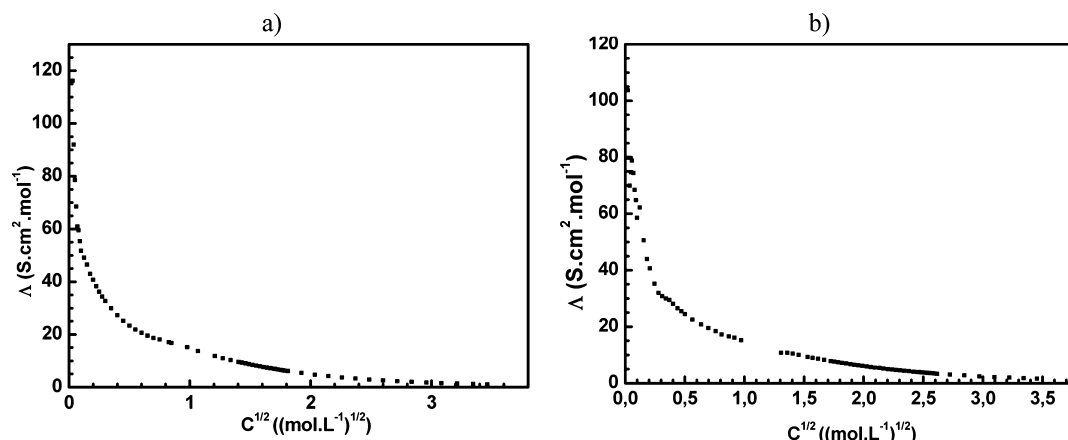


Figure 6. Debye–Onsager plot for (a) $[S_{111}][TFSI] + \gamma\text{-BL}$ and (b) $[HN_{111}][TFSI] + \gamma\text{-BL}$ at 298.15 K.

$$\Lambda \text{ (S} \cdot \text{cm}^2 \cdot \text{mol}^{-1}) = 1000 \left(\frac{\sigma}{C_{\text{IL}}} \right) \quad (3)$$

The increase in the molar conductance of solutions of strong electrolytes, with dilution, is mainly due to the increased mobility of the ions. Increases in dilution result in a decrease of inter-ions interactions, thereby increasing the migration speed of the ions, and hence the equivalent conductivity. The conductance behavior of strong electrolytes has been given by the Debye–Hückel–Onsager equation:

$$\Lambda = \Lambda^0 + (a\Lambda^0 + b)\sqrt{C_{\text{IL}}} \quad (4)$$

where Λ is the molar conductivity; Λ^0 , the infinite dilution molar conductivity; C_{IL} , the IL molar concentration; and a , b , two empirical constants. To determine the infinite dilution conductances of the ILs, the molar conductivity Λ versus $\sqrt{C_{\text{IL}}}$ was extrapolated to low IL concentrations. For these concentrations, Λ versus $\sqrt{C_{\text{IL}}}$ can be fitted by using a linear equation, as expected from the infinite dilution electrolyte type behavior,⁵⁶ based on the Debye–Onsager relationship.

The dependence of the molar conductivity, Λ , on the square root of the IL molar concentration, $\sqrt{C_{\text{IL}}}$ (C_{IL} in $\text{mol} \cdot \text{L}^{-1}$), according to the Debye–Onsager law (eq 4) is illustrated in Figure 6 in the case of $[S_{111}][TFSI] + \gamma\text{-BL}$ (Figure 6a) and $[HN_{111}][TFSI] + \gamma\text{-BL}$ (Figure 6b) at 298.15 K. From these graphs, we observed that, at IL concentrations higher than $C_{\text{IL}} > 1.0 \text{ mol} \cdot \text{L}^{-1}$, Λ decreases exponentially when C_{IL} increases. This behavior is characteristic of a weak electrolyte, partially associated in the solvent. The infinite dilution molar conductivities of both ILs, Λ^0 , presented in Table 3 were determined by fitting the experimental data by using eq 4 for all binary mixtures studied, herein.

In order to assess the influence of the temperature on the conductivity of each electrolyte, the conductivity of the mixture at the solvent mole fraction corresponding to the maximum conductivity at 298.15 K has been measured between 263.15 and 353.15 K. As expected, and shown in Figure 7, the conductivity increases with temperature and, in the case of ACN solutions with $[S_{111}][TFSI]$ (Figure 7a) and $[HN_{111}][TFSI]$ (Figure 7b), conductivities of 80 and 100 $\text{mS} \cdot \text{cm}^{-1}$ were obtained at 353.15 K, respectively. Interestingly, exceptionally high residual conductivity values of 35 and 42 $\text{mS} \cdot \text{cm}^{-1}$ were measured at low temperature, e.g., 263.15 K, in the case of ACN solutions with $[S_{111}][TFSI]$ and with $[HN_{111}][TFSI]$, respectively. These values could be attributed to the particularity of studied IL

Table 3. Calculated Molar Conductivities of Investigated ILs, Λ^0 (ILs), at Infinite Dilution from Conductivity Measurements for Studied Mixtures of ILs in $\gamma\text{-BL}$, PC, or ACN at 298.15 K, Where σ_{max} and $x_{\text{s(max)}}$ Are the Conductivity and the Solvent Mole Fraction at the Maximum Conductivity Reported for Each Solution Studied at 298.15 K

system	σ_{max} ($\text{mS} \cdot \text{cm}^{-1}$)	$x_{\text{s(max)}}$	Λ^0 (ILs) ($\text{S} \cdot \text{cm}^2 \cdot \text{mol}^{-1}$)
$[HN_{111}][TFSI] + \text{ACN}$	68.2	0.87	500
$[HN_{111}][TFSI] + \gamma\text{-BL}$	24.4	0.80	110
$[HN_{111}][TFSI] + \text{PC}$	16.66	0.76	50
$[S_{111}][TFSI] + \text{ACN}$	57.6	0.86	550
$[S_{111}][TFSI] + \gamma\text{-BL}$	20.1	0.74	130
$[S_{111}][TFSI] + \text{PC}$	13.95	0.70	160

structures driven by crystal plastic characteristics as discussed below.

One way of assessing the ionicity of the ionic liquids is to use the classification diagram based on the classical Walden rule.⁵⁷ The Walden rule relates the ionic mobility represented by the equivalent conductivity Λ to the fluidity η^{-1} of the medium through which the ions move. Figure 8 shows the Walden plots for the investigated mixtures. These plots were consistently localized below the “ideal” KCl line.⁵⁸ Furthermore, in each case, the slope, m_i , of each Walden plot, $\log(\Lambda)$ vs $\log(\eta^{-1})$, ranged from 0.75 to 0.87, indicating that each mixture has a subionic behavior;⁵⁹ this result can also be linked to the existence of tight ion pairs in solution, which do not undergo significant separation under the influence of an electric field and, therefore, do not contribute to ion current.

2.2. Fitting Procedure. The temperature dependence from 263.15 to 353.15 K on the conductivity and on the viscosity for each optimal composition studied, herein, is presented in Figures 9 and 10, respectively. These temperature dependences do not follow the Arrhenius law (eq 5) but are correctly fitted by using the Vogel–Tamman–Fulcher, VTF, equation (eq 6).

$$\sigma = \sigma_0 \exp \left[\frac{-E_a^\sigma}{(RT)} \right] \quad \eta = \eta_0 \exp \left[\frac{E_a^\eta}{(RT)} \right] \quad (5)$$

$$\sigma = \sigma_0 \exp \left[\frac{-B_\sigma}{(T - T_0)} \right] \quad \eta = \eta_0 \exp \left[\frac{B_\eta}{(T - T_0)} \right] \quad (6)$$

where η_0 , σ_0 , B_η , B_σ ($B_i = E_a/R$), and T_0 are the VTF fitting constants. The best-VTF fitting parameters for the viscosity and

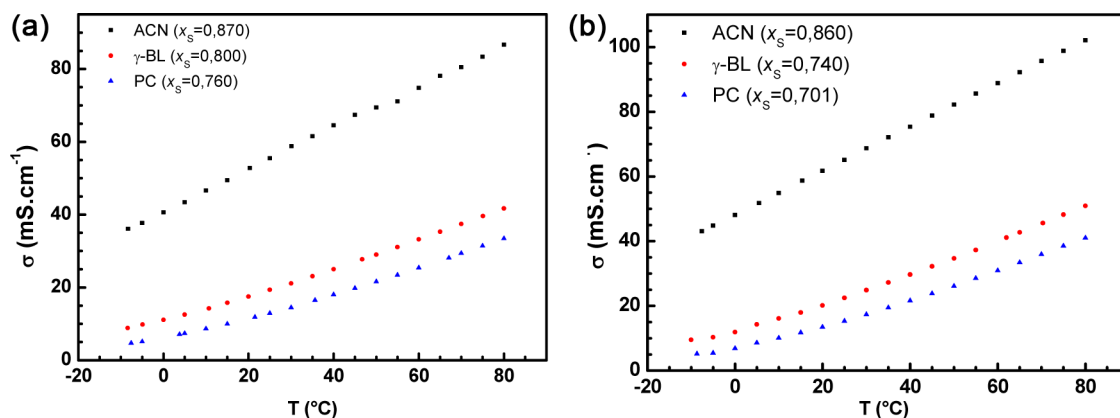


Figure 7. Conductivity of (a) $[S_{111}][TFSI]$ and (b) $[HN_{111}][TFSI]$ in a mixture with (■) ACN, (●) γ -BL, and (▲) PC as a function of the temperature at the solvent mole fraction corresponding to the maximum in the conductivity for each mixture at 298.15 K.

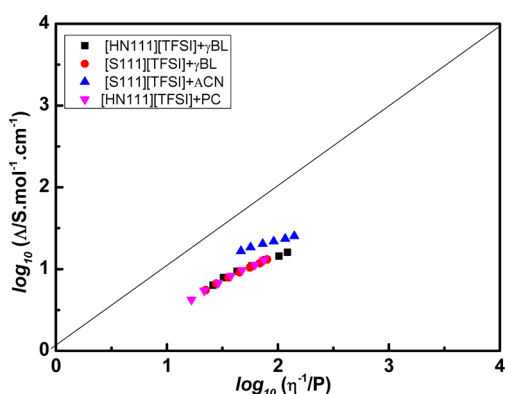


Figure 8. Walden plot for the investigated (IL + molecular solvent) binary systems.

conductivity as a function of temperature are reported in Table 4, together with the correlation coefficient for the fit.

B_η and B_σ are pseudo-activation energies ($B_i = E_a/R$) and can be linked to the energy barrier that needs to be overcome for the IL ions to move past each other with its solvent crown. Moreover, its value can be correlated with the structure of the IL and solvent structures.⁴⁰ From this point of view, the smaller the E_a value, the higher the viscosity and the conductivity of the electrolyte

solution, i.e. small E_a values enhance the ion mobility in solution. For both ILs, the pseudo-activation energy values for the ionic conduction process, E_a^σ , are in the order γ -BL > PC > ACN (see Table 4). Moreover, the E_a values for solution containing the sulfonium AIL are systematically smaller than those obtained for the ammonium PIL.

2.3. Thermal Properties of Selected ILs and Mixtures.

2.3.1. Thermal Stability of Selected ILs and Mixtures. The thermal behavior of ILs studied was investigated using DSC from -50 to 300 °C. Figure 11 shows the different phase transitions for pure ILs, from which the characteristic temperatures and enthalpies are deduced and listed in Table 5. During each DSC measurement, the sample was heated from 30 to 80 °C at 5 °C·min⁻¹ and then cooled from 80 to -60 °C. Thereafter, the sample was maintained at -60 °C for 3 min, and then heated to 300 °C at 5 °C·min⁻¹. Finally, each DSC sample was cooled from 300 to 30 °C at 5 °C·min⁻¹. In the case of mixtures with ACN, the vapor pressure of each mixture does not allow the measurements in this condition and is not reported, herein.

In the inset of Figure 11a, the heating cycles 1 and 2 show similar melting and eutectic temperatures characteristic of the presence of a residual water (1000 ppm) in the AIL as reported in our previous work.⁶⁰ No peak is observed between the melting point of each pure IL: $T_m = 49.28$ and 84.20 °C for $[S_{111}][TFSI]$ (Figure 11a) and $[HN_{111}][TFSI]$ (Figure 11b), respectively, and

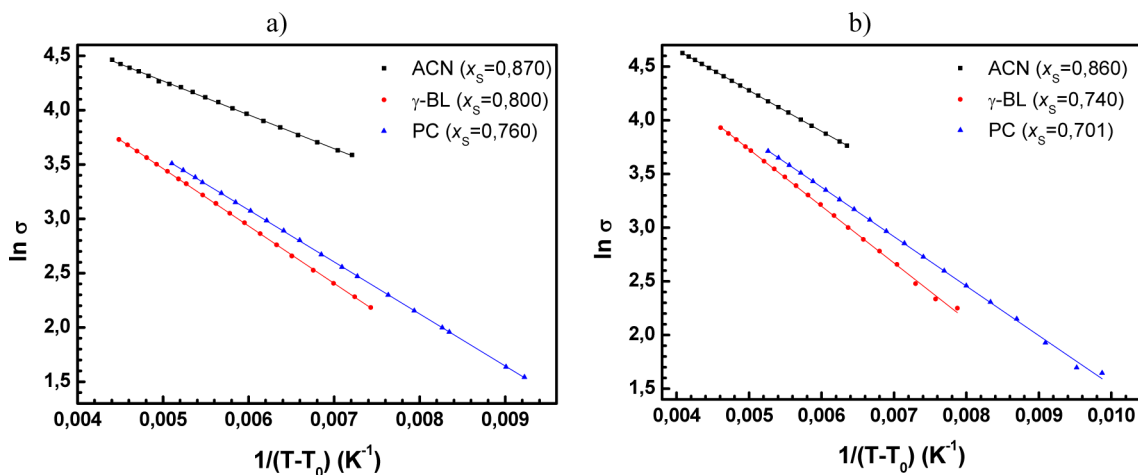


Figure 9. VTF plot for the conductivity of (a) $[S_{111}][TFSI]$ and (b) $[HN_{111}][TFSI]$ in a mixture with (■) ACN, (●) γ -BL, and (▲) PC as a function of the temperature at the solvent mole fraction corresponding to the maximum of the conductivity for each mixture at 298.15 K.

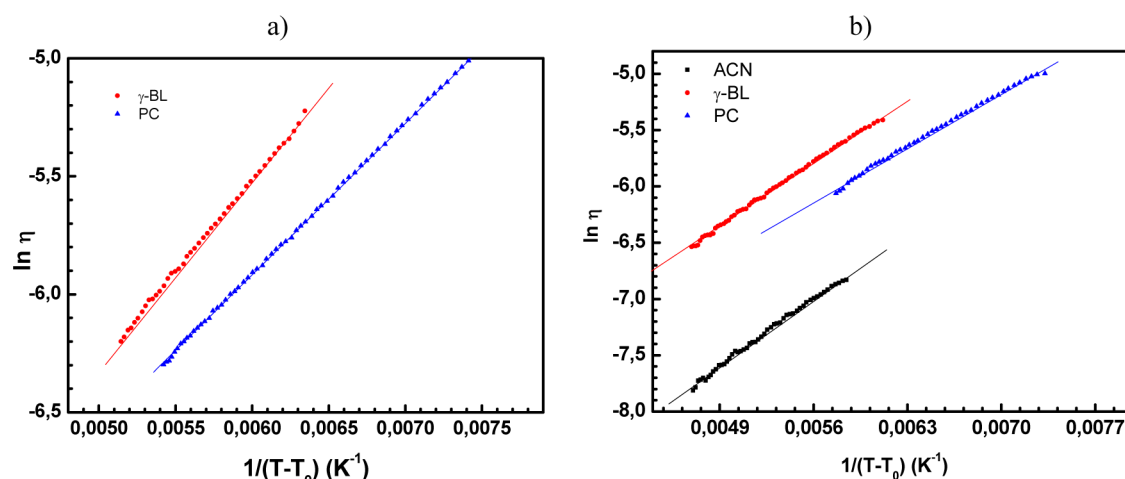


Figure 10. VTF plot for the viscosity of (a) $[S_{111}][TFSI]$ and (b) $[HN_{111}][TFSI]$ in a mixture with (■) ACN, (●) γ -BL, and (▲) PC as a function of the temperature at the solvent mole fraction corresponding to the maximum of the conductivity for each mixture at 298.15 K.

Table 4. Fitting VTF Parameters for the Temperature Dependences on the Conductivity and on the Viscosity of $[S_{111}][TFSI]$ and $[HN_{111}][TFSI]$ in a Mixture with ACN, γ -BL, or PC as a Function of the Temperature at the Solvent Mole Fraction Corresponding to the Maximum of the Conductivity for Each Mixture at 298.15 K (R^2 is the Correlation Coefficient of Each Fit)

T_0 (K)	$[S_{111}][TFSI]$			$[HN_{111}][TFSI]$		
	+ γ -BL	+ PC	+ ACN	+ γ -BL	+ PC	+ ACN
	130	157	126	136	163	108
σ_0 (mS·cm ⁻¹)	447.53	385.00	338.82	586.05	465.12	480.99
E_a^σ (kJ·mol ⁻¹)	4.39	3.98	2.59	4.40	3.83	3.16
R^2	0.9999	0.9999	0.9994	0.9991	0.9990	0.9999
$10^2 \times \eta_0$ (mPa·s)	3.03	2.43	0.77	2.54	5.73	
E_a^η (kJ·mol ⁻¹)	6.86	6.52	7.09	7.03	5.33	
R^2	0.9980	0.9906	0.9957	0.9961	0.9995	

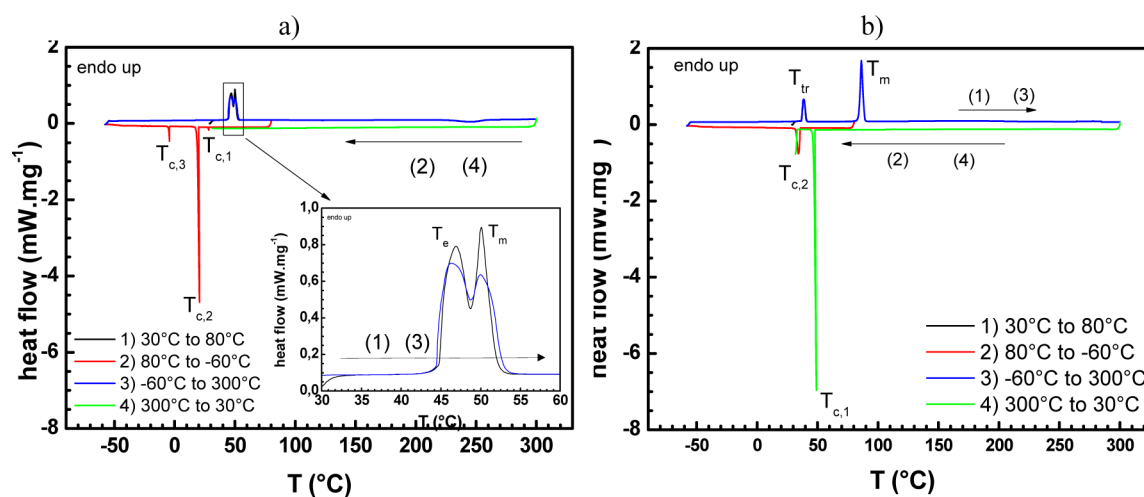


Figure 11. DSC thermograms for pure (a) $[S_{111}][TFSI]$ and (b) $[HN_{111}][TFSI]$ between -60 and 300 °C.

300 °C showing no significant decomposition, for example. The thermograms of both ILs show numerous peaks corresponding to different crystallization phases below the melting points. For example, three crystallization peaks, T_c , are observed between -4.3 and 28.4 °C with corresponding entropies, ΔS_c , of -0.49 , -50.22 , and -2.71 J·mol⁻¹·K⁻¹ in the case of the $[S_{111}][TFSI]$ (Figure 11a with values reported in Table S). In the case of the pure $[HN_{111}][TFSI]$ (Figure 11b with values reported in Table S), two crystallization peaks, T_c , are observed between 20.42 and 47.83 °C with corresponding entropies, ΔS_c , of -50.22 and

-3.32 J·mol⁻¹·K⁻¹, with a range of supercooled states up to 40 °C. For each IL, the observed crystallization peaks indicate also a strong organizational structure with many possible conformations corresponding to several solid–solid phase transitions T_{s-s} . This behavior is well described in the case of the trimethyl-sulfonium bis[fluoromethylsulfonyl]imide, $[S_{111}][FSI]$, and dimethyl-ethyl-sulfonium bis[fluoromethylsulfonyl]imide, $[S_{112}][FSI]$, salts, which are both solids at room temperature and exhibit solid–solid transitions at temperatures close to 8 °C, as well as an extremely low crystallization entropy, $\Delta S_c < 9$

Table 5. Thermal Properties of Pure $[S_{111}][TFSI]$ and $[HN_{111}][TFSI]$ ILs and of Their Mixtures with Each Investigated Solvent: Melting Point, T_m ($^{\circ}C$); Melting Enthalpy, ΔH_m ($kJ \cdot mol^{-1}$); Crystallization Temperature, T_c ($^{\circ}C$); Crystallization Enthalpy, ΔH_c ($kJ \cdot mol^{-1}$); Crystallization Entropy, ΔS_c ($J \cdot mol^{-1} \cdot K^{-1}$); Boiling Temperature, T_b ($^{\circ}C$); and Isobaric Heat Capacity, C_p ($J \cdot mol^{-1} \cdot K^{-1}$)

	T_c	T_m	T_b	ΔH_c	ΔH_m	ΔH_b	ΔS_c	C_p
$[S_{111}][TFSI]$	28.40			-0.15			-0.49	(-40 $^{\circ}C$) 291.57
	20.03	49.28		-14.72	53		-50.22	(25 $^{\circ}C$) 367.64
	-4.26			-0.73			-2.71	(100 $^{\circ}C$) 378.90
$[HN_{111}][TFSI]$								(-40 $^{\circ}C$) 282.52
	47.83	84.20		-17.20	17.36		-53.60	(25 $^{\circ}C$) 329.68
	20.42						-3.32	(100 $^{\circ}C$) 355.12
$([S_{111}][TFSI] + \gamma\text{-BL})$								(-40 $^{\circ}C$) 147.57
	0.5		220.37			22.70		(25 $^{\circ}C$) 190.85
								(100 $^{\circ}C$) 233.50
$([HN_{111}][TFSI] + \gamma\text{-BL})$								(-40 $^{\circ}C$) 398.62
	49.2		223.93			21.09		(25 $^{\circ}C$) 412.18
								(100 $^{\circ}C$) 451.06
$([S_{111}][TFSI] + PC)$								(-40 $^{\circ}C$) 427.35
			233.73			19.93		(25 $^{\circ}C$) 447.40
								(100 $^{\circ}C$) 505.97
$([HN_{111}][TFSI] + PC)$								(-40 $^{\circ}C$) 389.35
	48.4		228.61			21.24		(25 $^{\circ}C$) 379.88
								(100 $^{\circ}C$) 495.14

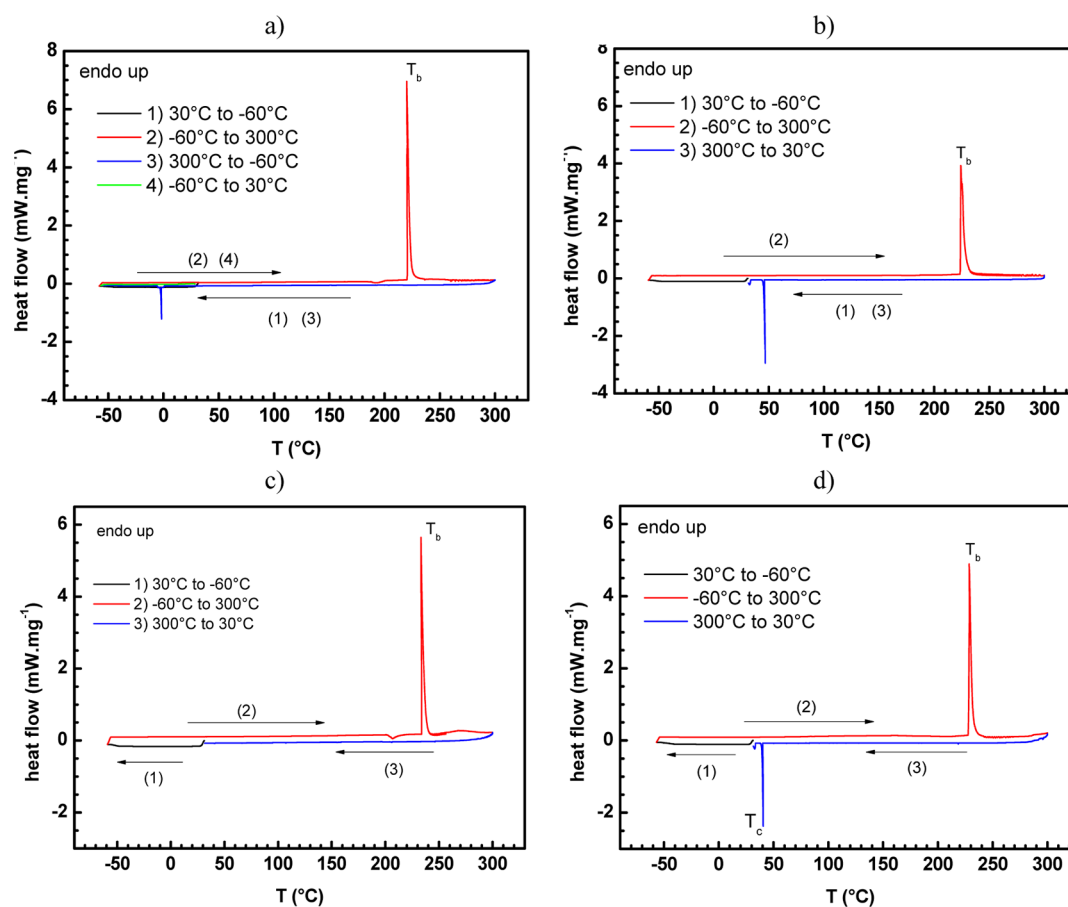


Figure 12. DSC thermograms of (a) $[S_{111}][TFSI] + PC$, (b) $[HN_{111}][TFSI] + PC$, (c) $[S_{111}][TFSI] + \gamma\text{-BL}$, and (d) $[HN_{111}][TFSI] + \gamma\text{-BL}$ as a function of the temperature from -60 to 300 $^{\circ}C$ at the solvent mole fraction corresponding to the maximum of the conductivity for each mixture at 298.15 K.

$J \cdot mol^{-1} \cdot K^{-1}$.⁶¹ These materials are classified as plastic crystals and are interesting as ambient-temperature solid electrolytes.^{62,63}

The thermograms reported in Figure 12 show that the mixtures of both ILs + PC (Figure 12a and b) and ILs + $\gamma\text{-BL}$ (Figure 12c and d) binary mixtures remain thermally stable up to

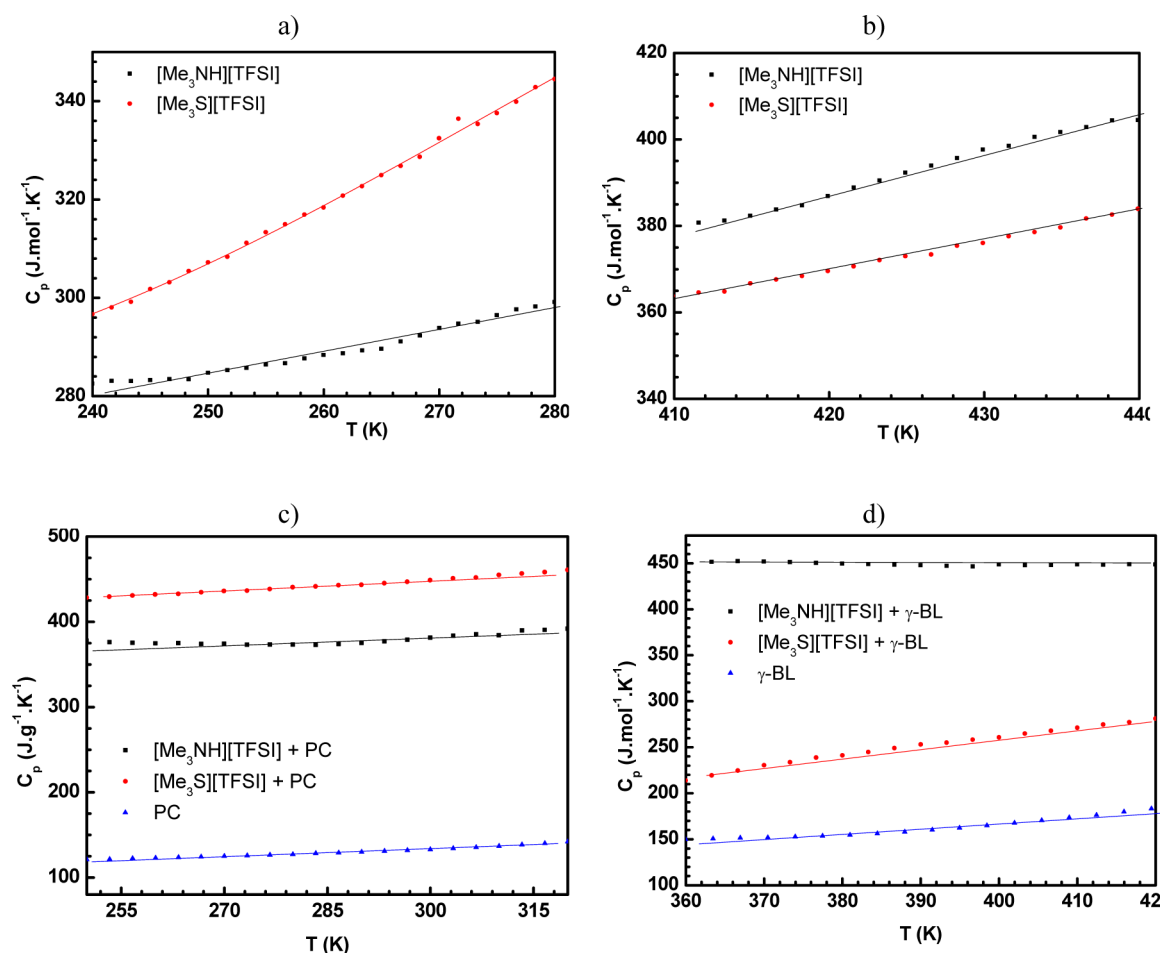


Figure 13. Molar heat capacities, C_p , as a function of the temperature of (a) pure $[S_{111}][TFSI]$ and $[HN_{111}][TFSI]$ at low temperature from 240 to 280 K, (b) pure $[S_{111}][TFSI]$ and $[HN_{111}][TFSI]$ at high temperature from 410 to 440 K, (c) $[S_{111}][TFSI]$ + PC and $[HN_{111}][TFSI]$ + PC binary mixtures from 255 to 315 K, and (d) $[S_{111}][TFSI]$ + γ -BL and $[HN_{111}][TFSI]$ + γ -BL binary mixtures from 360 to 420 K.

temperatures close to the boiling temperature of the pure investigated solvents, e.g., 220 and 230 °C in the case of γ -BL and PC solutions, respectively. The exothermic peaks observed during each cooling rate from 300 to -60 °C correspond to the crystallization of each mixture; e.g., $T_c \approx 47$ °C is observed in the case of solutions containing the $[HN_{111}][TFSI]$ and PC (Figure 12b) or γ -BL (Figure 12d), and $T_c \approx 0$ °C was obtained in the case of the $[S_{111}][TFSI]$ + γ -BL binary mixture (Figure 12c). In the case of $[S_{111}][TFSI]$ + PC solutions, no crystallization was observed, as shown in Figure 12a and Table 5. Furthermore, this binary mixture remains in a liquid state at very low temperature, lower than -60 °C, which is the temperature limit of our equipment. This behavior is interesting from the perspective of low temperature devices.

2.3.2. Specific Heat Capacities of Selected ILs and Mixtures.

Molar heat capacities, C_p , of the two ILs studied and selected mixtures are shown in Figures 13 as a function of temperature. In each case, the calculated C_p at -40 , 25, and 100 °C are summarized in Table 5. As expected, in each case, C_p increases linearly with temperature. Furthermore, $[S_{111}][TFSI]$ has higher C_p values than $[HN_{111}][TFSI]$ at low temperature (Figure 13a); this tendency is reversed at high temperature (Figure 13b). This tendency could be explained by the difference observed between their T_c and T_m , as well as the temperature effect on their thermal behavior.

The molar heat capacities, C_p , of binary solutions containing the $[S_{111}][TFSI]$ and $[HN_{111}][TFSI]$ mixed with PC or γ -BL have been measured under standard pressure at the solvent weight fraction composition, $w_s \approx 0.5$, over the temperature range from 250 to 320 K and from 360 to 420 K in the case of the PC and γ -BL solutions, respectively. The C_p values obtained and the corresponding mean standard deviations are tabulated in Table 5. The results show that, for all the investigated mixtures, C_p increases slightly with temperature. The C_p obtained in the case of the $[HN_{111}][TFSI]$ + γ -BL binary system was found to be relatively constant over the temperature covered in this study. It is also clearly shown in Figure 13 that the C_p values of pure ILs are higher than those obtained in the case of the pure molecular solvents, PC (Figure 13c) and γ -BL (Figure 13d), and lower than the calculated C_p values of each binary system with the exception of the $[S_{111}][TFSI]$ + γ -BL solution. These observations are due to the dependence of C_p on the number of translational, vibrational, and rotational energy storage modes in the molecules, as well as the fact that ILs have higher molecular weights than the pure molecular solvents or than their mixture with ILs.⁶⁴

CONCLUSIONS

The thermophysical properties of two homologous ILs, namely, $[S_{111}][TFSI]$ and $[HN_{111}][TFSI]$ in their pure form and in mixtures with PC, ACN, and γ -BL, were investigated through a

comparative study. The influence of the addition of ACN, γ -BL, and PC on the viscosity, conductivity, and thermal properties was investigated for different molar fractions of the solvent from the IL solid solubility limit in each solvent to the pure solvent at several temperatures. The effect of temperature on the conductivities and viscosities for investigated binary mixtures was determined by fitting the experimental data at the solvent mole fraction corresponding to the maximum conductivity for each mixture at 298.15 K from 263.15 to 353.15 K. These measurements show residual conductivity at low temperature, 263.15 K, with exceptionally high values of up to 35 and 42 mS·cm⁻¹ in the case of the ACN solutions containing the [S₁₁₁][TFSI] and [HN₁₁₁][TFSI], respectively. In addition, a theoretical approach linking the conductivity and the viscosity of electrolytes has been formulated by treating the migration of the ions as a dynamical process governed by ion–ion and solvent–ion interactions within a prior viscosity data analysis by using the Jones–Dole equation. From this model, the calculated conductivity data as a function of the composition up to the IL saturation limit in each solvent was found to be in good agreement with experimental values. The thermal properties of each selected IL and the binary mixtures have been analyzed by using different heating/cooling DSC scans. The DSC results show the existence of many crystallization peaks corresponding to different solid–solid phase transitions, T_{s-s} , with extremely low melting entropy, indicating a strong organizational structure. From this data, these ILs can be classified as plastic crystals and are promising for use in mixtures with ACN as ambient-temperature solid electrolytes, as well as classical electrolytes in mixtures with molecular solvents such as PC or γ -BL at temperatures up to ~200 °C.

■ ASSOCIATED CONTENT

■ Supporting Information

¹H and ¹³C NMR spectra of each pure IL investigated in this work are provided in Figures S1 and S2. Viscosity and conductivity data of pure ILs and selected mixtures as a function of composition and of the temperature are tabulated in Tables S1–S3 and visualized in Figures S3–S5. This material is available free of charge via the Internet at <http://pubs.acs.org>.

■ AUTHOR INFORMATION

Corresponding Author

*E-mail: meriem.anouti@univ-tours.fr. Fax: (33)247367360. Phone: (33)247366951.

Notes

The authors declare no competing financial interest.

■ REFERENCES

- (1) Welton, T. *Chem. Rev.* **1999**, *99*, 2071–2084.
- (2) Greaves, T. L.; Drummond, C. J. *Chem. Rev.* **2008**, *108*, 206–237.
- (3) Wasserscheid, P.; Keim, W. *Angew. Chem., Int. Ed.* **2000**, *39*, 3772–3789.
- (4) Attri, P.; Reddy, P. M.; Venkatesu, P.; Kumar, A.; Hofman, T. J. *Phys. Chem. B* **2010**, *114*, 6126–6133.
- (5) Wang, C.; Cui, G.; Luo, X.; Xu, Y.; Li, H.; Dai, S. *J. Am. Chem. Soc.* **2011**, *133*, 11916–11919.
- (6) Attri, P.; Venkatesu, P.; Kumar, A. *J. Phys. Chem. B* **2010**, *114*, 13415–13425.
- (7) Plechkova, N. V.; Seddon, K. R. *Chem. Soc. Rev.* **2008**, *37*, 123–150.
- (8) Minami, I. *Molecule* **2009**, *14*, 2286–2305.
- (9) Hough, W. L.; Rogers, R. D. *Bull. Chem. Soc. Jpn.* **2007**, *80*, 2262–2269.
- (10) Hough, W. L.; Smiglak, M.; Rodriguez, H.; Swatloski, R. P.; Spear, S. K.; Daly, D. T.; Pernak, J.; Grisel, J. E.; Carliss, R. D.; Soutullo, M. D.; Davis, J. J. H.; Rogers, R. D. *New J. Chem.* **2007**, *31*, 1429–1436.
- (11) MacFarlane, D. R.; Forsyth, M.; Howlett, P. C.; Pringle, J. M.; Sun, J.; Annat, G.; Neil, W.; Izgorodina, E. I. *Acc. Chem. Res.* **2007**, *40*, 1165–1173.
- (12) Dupont de Souza, J. R. F.; Suarez, P. A. Z. *Chem. Rev.* **2002**, *102*, 3667–3692.
- (13) Blanchard, L. A.; Hancu, D.; Beckman, E. J.; Brennecke, J. F. *Nature* **1999**, *399*, 28–29.
- (14) Hagiwara, R.; Ito, Y. *J. Fluorine Chem.* **2000**, *105*, 221–227.
- (15) Eastoe, J.; Gold, S.; Rogers, S. E.; Paul, A.; Welton, T.; Heenan, R. K.; Grillo, I. *J. Am. Chem. Soc.* **2005**, *127*, 7302–7303.
- (16) He, Y.; Li, Z.; Simone, P.; Lodge, T. P. *J. Am. Chem. Soc.* **2006**, *128*, 2745–2750.
- (17) Kim, K.-S.; Choi, S.; Dembereinyamba, D.; Lee, H.; Oh, J.; Lee, B.-B.; Mun, S.-J. *Chem. Commun.* **2004**, 828–829.
- (18) Xu, W.; Angell, C. A. *Science* **2003**, *302*, 422–425.
- (19) Yoshizawa, M.; Xu, W.; Angell, C. A. *J. Am. Chem. Soc.* **2003**, *125*, 15411–15419.
- (20) Greaves, T. L.; Weerawardena, A.; Fong, C.; Krodziewska, I.; Drummond, C. J. *J. Phys. Chem. B* **2006**, *110*, 22479–22487.
- (21) Atkin, R.; Warr, G. G. *J. Phys. Chem. B* **2008**, *112*, 4164–4166.
- (22) Greaves, L. T.; Kennedy, D. F.; Mudie, S. T.; Drummond, C. J. *J. Phys. Chem. B* **2010**, *114*, 10022–10031.
- (23) Araos, M. U.; Warr, G. G. *J. Phys. Chem. B* **2005**, *109*, 14275–14277.
- (24) Anouti, M.; Jones, J.; Boisset, A.; Jacquemin, J.; Caillon-Caravanier, M.; Lemordant, D. *J. Colloid Interface Sci.* **2009**, *340*, 104–111.
- (25) Janus, E.; Goc-Maciejewska, I.; Lozynski, M.; Pernak, T. *Tetrahedron Lett.* **2006**, *47*, 4079–4083.
- (26) Zhao, G. Y.; Jiang, T.; Gao, H. X.; Han, B. X.; Huang, J.; Sun, D. H. *Green Chem.* **2004**, *6*, 75–77.
- (27) Angell, C. A.; Wang, L. M. *Biophys. Chem.* **2003**, *105*, 621–367.
- (28) Lau, R. M.; Sorgedraeger, M. J.; Carrea, G.; van Rantwijk, F.; Secundo, F.; Sheldon, R. *Green Chem.* **2004**, *6*, 483–487.
- (29) Noda, A.; Susan, A. B.; Kudo, K.; Mitsushima, S.; Hayamizu, K.; Watanabe, M. *J. Phys. Chem. B* **2003**, *107*, 4024–4033.
- (30) Sun, J. Z.; Jordan, L. R.; Forsyth, M.; MacFarlane, D. R. *Electrochim. Acta* **2001**, *46*, 1703–1708.
- (31) Gutowski, K. E.; Holbrey, J. D.; Rogers, R. D.; Dixon, D. A. *J. Phys. Chem. B* **2005**, *109*, 23196–23208.
- (32) Paulsson, H.; Berggrund, M.; Svantesson, E.; Hagfeldt, A.; Kloo, L. *Sol. Energy Mater. Sol. Cells* **2004**, *82*, 345–360.
- (33) Wang, P.; Wenger, B.; Humphry-Baker, R.; Moser, J.-E.; Teuscher, J.; Kuntlehner, W.; Mezger, J.; Stoyanov, E. V.; Zakeeruddin, S. M.; Grätzel, M. *J. Am. Chem. Soc.* **2005**, *127*, 6850–6856.
- (34) Paulsson, H.; Hagfeldt, A.; Kloo, L. *J. Phys. Chem. B* **2003**, *107*, 13665–13670.
- (35) Gerhard, D.; Alpaslan, S. C.; Gores, H. J.; Uerdingen, M.; Wasserscheid, P. *Chem. Commun.* **2005**, 5080–5082.
- (36) Watanabe, M.; Mizumura, T. *Solid State Ionics* **1996**, *86–88*, 353–356.
- (37) Noda, A.; Hayamizu, K.; Watanabe, M. *J. Phys. Chem. B* **2001**, *105*, 4603–4610.
- (38) Lewandowski, A.; Galinski, M. *J. Phys. Chem. Solids* **2004**, *65*, 281–286.
- (39) Anouti, M.; Jacquemin, J.; Porion, P. *J. Phys. Chem. B* **2012**, *116*, 4228–4238.
- (40) Okoturo, T. J.; VanderNoot, J. *Electroanal. Chem.* **2004**, *568*, 167–181.
- (41) Tao, G.-H.; He, L.; Sun, N.; Kou, Y. *Chem. Commun.* **2005**, 3562–3564.
- (42) Fang, S.; Yang, L.; Wei, C.; Peng, C.; Tachibana, K.; Kamijima, K. *Electrochem. Commun.* **2007**, *9*, 2696–2702.
- (43) Han, H.-B.; Nie, J.; Liu, K.; Li, W.-K.; Feng, W.-F.; Armand, M.; Matsumoto, H.; Zhou, Z.-B. *Electrochim. Acta* **2010**, *55*, 1221–1226.

- (44) Timperman, L.; Skowron, P.; Boisset, A.; Galiano, H.; Lemordant, D.; Frackowiak, E.; Béguin, F.; Anouti, M. *Phys. Chem. Chem. Phys.* **2012**, *14*, 8199–8207.
- (45) Anouti, M.; Caillon-Caravanier, M.; Dridi, Y.; Galiano, H.; Lemordant, D. *J. Phys. Chem. B* **2008**, *112*, 13335–13343.
- (46) Jones, G.; Dole, M. *J. Am. Chem. Soc.* **1929**, *51*, 2950–2964.
- (47) Hribar, B. N.; Southall, T.; Vlachy, V.; Dill, K. A. *J. Am. Chem. Soc.* **2002**, *124*, 12302–12311.
- (48) Vila, J.; Gines, P.; Rilo, E.; Cabeza, O.; Varela, L. M. *Fluid Phase Equilib.* **2006**, *247*, 32–39.
- (49) Jarosik, A.; Krajewski, S. R.; Lewandowski, A.; Radzimski, P. *J. Mol. Liq.* **2006**, *123*, 43–50.
- (50) Claes, P.; Loix, Y.; Glibert, J. *Electrochim. Acta* **1983**, *28*, 421–428.
- (51) Vila, J.; Rilo, E.; Segade, L.; Cabeza, O.; Varela, L. M. *Phys. Rev.* **2005**, *E 71* (3), 031201-1–031201-8.
- (52) Bockris, J. O'M.; Reddy, A. K. N. *Modern Electrochemistry*; Plenum Press: New York, 1998; Vol. 1.
- (53) Chandra, A.; Bagchi, B. *J. Chem. Phys.* **1999**, *110*, 10024–10034.
- (54) Horvath, A. L. *Aqueous Electrolyte Solutions: Physical Properties, Estimation, and Correlation Methods*; Ellis Horwood: London, 1985.
- (55) Villullas, H. M.; Gonzalez, E. R. *J. Phys. Chem. B* **2005**, *109*, 9166–91673.
- (56) Robinson, R. A.; Stokes, R. H. *Electrolyte Solutions*; Butterworths: London, 1965.
- (57) Walden, P. *Z. Phys. Chem.* **1906**, *55*, 207, 246.
- (58) Schreiner, C.; Zugmann, S.; Hartl, R.; Gores, H. *J. Chem. Eng. Data* **2009**, *55*, 1784–1788.
- (59) Xu, W.; Cooper, E. I.; Angell, C. A. *J. Phys. Chem. B* **2003**, *107*, 6170–6178.
- (60) Anouti, M.; Timperman, L.; El Hilali, M.; Boisset, A.; Galiano, H. *J. Phys. Chem. C* **2012**, *116*, 9412–9418.
- (61) MacFarlane, D. R.; Huang, J.; Forsyth, M. *Nature* **1999**, *402*, 792–794.
- (62) MacFarlane, D. R.; Meakin, P.; Sun, J.; Amini, N.; Forsyth, M. *J. Phys. Chem. B* **1999**, *103*, 4164–4170.
- (63) Alarco, P.-J.; Abu-Lebdeh, Y.; Abouimrane, A.; Armand, M. *Nat. Mater.* **2004**, *3*, 476–481.
- (64) Crosthwaite, J. M.; Muldoon, M. J.; Dixon, J. K.; Anderson, J. L.; Brennecke, J. F. *J. Chem. Thermodyn.* **2005**, *37*, 559–568.